NUMERICAL CALCULATION AND ANALYSIS OF FSW PROCESS FOR HIGH STRENGTH 7075 ALUMINUM ALLOY BASED ON CEL METHOD

Yuanpeng LIU[1], Kun CHEN[1,2], Guang ZENG[1,*], Zhenghe WANG[1], Shuai TIAN[1], Kaishan NIE[1]

Taking 7075 aluminum alloy as the research object, considering the nonlinear influence of temperature change on material properties, The Johnson-Cook constitutive model is adopted to describe the thermodynamic properties of materials. Based on the Coupled Eulerian-Lagrangian (CEL) method, a 3D model of friction stir welding (FSW) process of 7075 aluminum alloy was constructed, and three stages of plunging, dwelling and welding were simulated by Thermodynamic coupling FE method. The influence of welding parameters on weld quality, temperature distribution and stress-strain was systematically studied. The results show that the temperature distribution during welding is asymmetrical, and the temperature of the retreating side is higher than that of the advancing side. The stress distribution is approximately symmetrical, but the distribution of PEEQ on the inner and outer sides of the shoulder stirring zone is uneven. After some materials reach thermoplasticity, it is difficult to further increase the temperature by increasing the rotating speed. However, the effect of reducing welding speed on increasing temperature is significant. The numerical results are in good agreement with the experimental results, which shows the correctness of the model. When the rotating speed is 1200mm/min and the welding speed is 144mm/min, the highest temperature reaches more than 93% of the melting point of the material, the welding defects are reduced and the weld forming quality is excellent.

Key words: Aluminum alloy, FSW, CEL, Temperature, Numerical Calculation.

1. Introduction

Common aluminum alloys are prone to oxidation after melting at high temperature, resulting in cracks, holes and oxide inclusions in welds. Friction stir welding (FSW), as a mature new "solid phase" welding technology, does not require metal filler and will not melt the material to be welded, especially suitable for welding low melting point metal materials such as aluminum alloys[1-3]. Different from traditional fusion welding, this kind of solid-state welding has less heat input, serious plastic deformation and high weld quality[4]. Friction between the stirring

[1] School of Aerospace Engineering, Zhengzhou University of Aeronautics, Zhengzhou, China, *e-mail:zengg8899@163.com (corresponding author)
[2] School of Materials Science and Engineering, Zhengzhou University of Aeronautics, Zhengzhou, China, e-mail:Lyp5599@126.com

tool and material and plastic deformation of the internal shear layer of the material are the main sources of welding heat[5]. The material around the stirring tool is heated to be thermoplastic, but it has not yet melted. Thermoplastic materials are stirred and cooled to form a mechanical interlock to achieve the purpose of welding. To solve the problem of serious defects in aluminum alloy welding by traditional methods, the FSW process can be successfully used because it can improve the quality of aluminum alloy welding, and has already been widely used in aerospace, rail transit, shipbuilding and other fields[6-8].

Andrade et al. studied the correlation law between torque and temperature and welding conditions in standard aluminum alloys AA 2xxx, 5xxx, 6xxx and 7xxx welded by the FSW process and found that the tool speed has an important influence on the heat generated during welding, which is an important factor which affects the quality of the weld[9]. Azhagar et al. studied the effect of stirring tool on heat transfer and material properties of FSW using two kinds of conical stirring tools with and without groove under the conditions of 1800r/min rotation speed and 50mm/min welding speed[10]. Milcic et al. conducted experiments on the influence of FSW process parameters of 6mm thick 2024-T351 aluminum alloy plate on the mechanical properties of the joint. The experimental results show that the mechanical properties of the weld are the best when the rotating speed and welding speed are 750r/min and 116mm/min, respectively[11]. In FSW process, the rotating speed of stirring tool, welding speed and the shape of stirring pin can all affect the fluidity and flow behavior of materials, and then affect the quality of weld formation. Through FSW process experiments with different welding parameters and different stirring pin shapes, we can find out a group of parameters with the best forming effect.

However, all the above studies are based on experiments. With the development of software technology, advanced numerical simulation analysis can simulate the material flow, temperature, stress-strain, deformation and defects in the welding process, which tends to replace some experimental requirements. In recent years, scholars in the industry have gradually increased their simulation research on FSW. Mostafa et al[12] simulated the FSW between AA5083 and AA7075 by using the CEL method, and studied the influence of welding speed and rotating speed on material flow, temperature and strain. Salloomi[13] improved the sequence modeling of FSW process by using ALE formula and analyzed the three stages of FSW process. The results show that the temperature is evenly distributed along the width of the “T” joint, and the temperature nephogram is “V” shaped in

the stirring zone, the plastic strain value on the advancing side is significantly higher than the plastic strain value on the retreating side. Hkammess[14] used FSW process to analyze the temperature distribution of AA2024-T3 and AA6061-T6 aluminum alloys by finite element (FE) method. It was found that when the welding speed was low, the increase of rotating speed had no effect on the welding temperature, and the lower surface temperature of the materials was symmetrically distributed, but it was low.

It should be noted that compared with other aluminum alloys, 7075 aluminum alloy has higher strength, but poor weldability and more expensive price. In order to obtain a good welded joint, researchers usually need to carry out a large number of experiments to adjust the welding parameters. Multi-thread calculation by digital simulation can creatively speed up the research on weldability of 7075 aluminum alloy, find the parameter range of defect-free FSW joint, and provide the basis for parameter selection for subsequent experiments. At present, there are few reports on FSW Euler simulation experiments of 7075 aluminum alloy in the field. In this study, 20-core CPU parallel workstations are used for welding simulation, which breaks the constraints of experimental conditions, equipment and material procurement. Moreover, the research flow is easier to realize. With the continuous innovation of numerical simulation methods, many branches have been derived. Common methods include but are not limited to Computational Fluid Dynamics (CFD)[15], Arbitrary Lagrangian-Euler method (ALE)[16] and Coupled Eulerian-Lagrangian (CEL) method[17]. Based on the CEL method, this paper simulates the FSW process, studies the variation law of temperature field, stress and strain in the three stages of plunging, dwelling and welding, analyzes the material flow phenomenon, and observes the formation of internal defects in the joint.

2. FSW thermodynamic coupling simulation model

2.1 Model building and grid division

CEL method can not only effectively predict the formation of welding defects, but also fix the grid while the material flows, thus avoiding excessive grid distortion in the simulation process[18]. As shown in Fig. 1(a), according to the basic principle of CEL method, a 40×50×7mm FE model is established in the coordinate system and set as Euler body. The model is divided into two layers: 4mm and 3mm along the direction perpendicular to the plate thickness, in which the 4mm part is the filling area of welding material, and the 3mm air layer is reserved for material flow space and absorbing flash. The FSW model stirring tool adopts a

classic cylindrical shape. The diameter of the stirring pin is 4mm, and the shoulder is 8mm. As shown in Fig. 1(b), in order to avoid stress concentration in the process of plunging and welding, the stirring tool adopts chamfer design. Moreover, in order to reduce the calculation difficulty and facilitate the simulation analysis, the rotation speed of stirring tool is considered to be constant, and its wear, deformation and fracture analysis are not considered, so it is set as a rigid body[19]. The Euler domain is meshed with the thermodynamic coupling element (EC3D8RT). When meshing the Euler domain, finer meshes are used in the main deformation area and sparser meshes are used in the periphery. This way can not only ensure the accuracy of material deformation in Euler domain, but also reduce the amount of calculation and shorten the calculation period. The stirring tool is meshed by an eight-node thermally coupled hexahedron element (C3D8T), and the results are shown in Fig. 1.

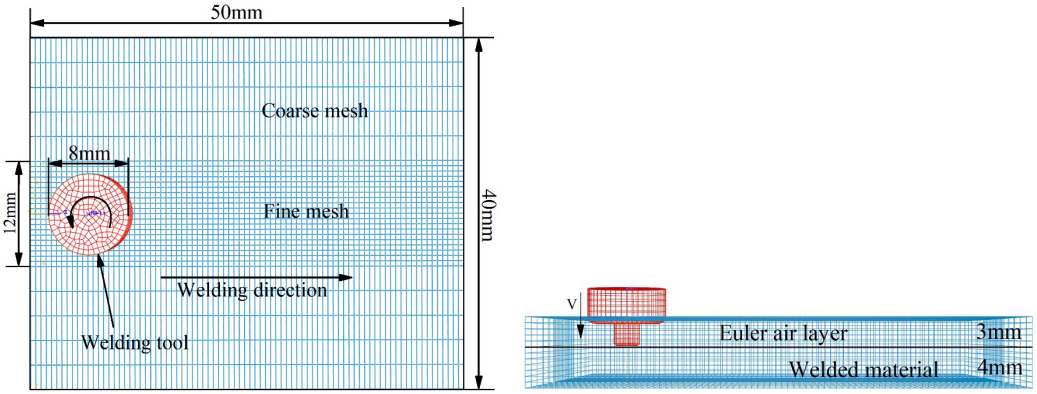

a) top view ***b***) side view

Fig. 1. Three-dimensional FE model and mesh generation

2.2 Material property model

In this study, the welded material is 7075 aluminum alloy, and the stirring tool is made of tool steel, which is set as a rigid body in the simulation. The main elements of 7075 aluminum alloy are as follows:

Table 1.

Chemical composition of 7075 aluminum plate[20]

wt%(Si)	wt%(Fe)	wt%(Cu)	wt%(Mn)	wt%(Mg)
< 0.40	< 0.50	1.2~2.0	< 0.30	2.1~2.9
wt%(Cr)	wt%(Zn)	wt%(Ti)	wt%(Al)	
0.18~0.28	5.1~6.1	0.20	Bal.	

FSW is a large deformation process. Considering the nonlinear influence of temperature change on material properties, Johnson-Cook constitutive model can describe the relationship between strain rate, strain and temperature as follows[21-22]:

$$\sigma = (A + B\bar{\varepsilon}_{pl}{}^{n})\left(1 + C\ln\frac{\dot{\bar{\varepsilon}}_{pl}}{\dot{\varepsilon}_0}\right)\left[1 - \left(\frac{T - T_{ref}}{T_{melt} - T_{ref}}\right)^{m}\right] \quad (1)$$

In the formula, $\bar{\varepsilon}_{pl}$ stands for equivalent plastic strain, $\dot{\bar{\varepsilon}}_{pl}$ refers to the equivalent plastic strain rate, $\dot{\varepsilon}_0$ means reference strain rate, T_{ref} is the ambient temperature, T_{melt} is the melting point of the 7075 aluminum alloy, "A, B, C, N and M" are all material constants, in which constants A, B and N are obtained by experiments at room temperature, and N stands for strain hardening effect, M represents high temperature softening effect, and C represents strain rate sensitivity[23]. Table 2 lists the parameters of J-C constitutive equation of 7075 aluminum alloy:

Table 2.

Parameters of J-C Constitutive Equation of 7075 Aluminum Alloy

A/MPa	B/MPa	C	n	m	T_{melt}	T_{ref}
441	383	0.0083	0.183	0.859	610	20

2.3 Boundary condition setting

The heat dissipation of the FSW process is generally considered to be carried out by thermal convection and thermal radiation on the side and upper surface of the plate. However, the radiation heat transfer process is complex, which can be converted into convection heat transfer for simulation, so it is necessary to set the thermal boundary condition and convection heat transfer coefficient on the surface of the material.

The expression of convective heat transfer is as follows (2):

$$Q_c = H_c(T_a - T) \quad (2)$$

In the formula, Q_c means the heat flux of convective heat transfer, T_a is the ambient temperature, H_c refers to the convective heat transfer coefficient, T stands for the surface temperature of the object.

The expression of radiation heat transfer is as follows (3):

$$Q_r = \sigma_b \varepsilon_b (T_a{}^4 - T^4) \quad (3)$$

In the formula, $\sigma_b = 5.67 \times 10^{-8}$ is Stefan-Boltzmann constant; ε_b is the surface blackness coefficient of the material.

Combined with formulas (2) and (3), the expression of the total heat transfer coefficient is shown in formula (4):

$$Q_t = \left[H_c + \sigma_b \varepsilon_b (T_a{}^2 - T^2)(T_a + T)\right](T_a - T) \quad (4)$$

The total heat transfer coefficient between material surface and air is:

$$H_t = H_c + \sigma_b \varepsilon_b (T_a{}^2 - T^2)(T_a + T) \quad (5)$$

So:

$$Q_t = H_t (T_a - T) \quad (6)$$

After debugging, the total heat transfer coefficient between material surface and air is set as $25W/(m^2 \cdot ℃)$ in this study. The lower surface of the plate is in direct contact with the fixed pad, which belongs to contact heat transfer. The contact heat transfer coefficient is influenced by the inherent properties of materials, contact pressure, temperature and contact state, so it is converted into convection heat transfer coefficient[24]. Considering the above reasons, in order to make this simulation closer to the real experimental situation, by debugging the software parameters, the heat transfer coefficient of the material bottom surface is finally set to $400W/(m^2 \cdot ℃)$.

As shown in fig.2, in order to prevent the plate moving or thermoplastic flowing of material in the Euler domain during welding, have been set boundary conditions in the model to limit the velocity and angular velocity of material plate in 'x' and 'z' directions, and the movement of the bottom surface of the plate in the negative direction of y-axis. The plunging time of the stirring pin is 1s, and the interference of shoulder pressed into the material is 0.1 mm. A reference point RP-1 is set at the intersection between the rotating axis of the stirring tool and the upper surface to determine the rotating motion trajectory of the stirring tool.

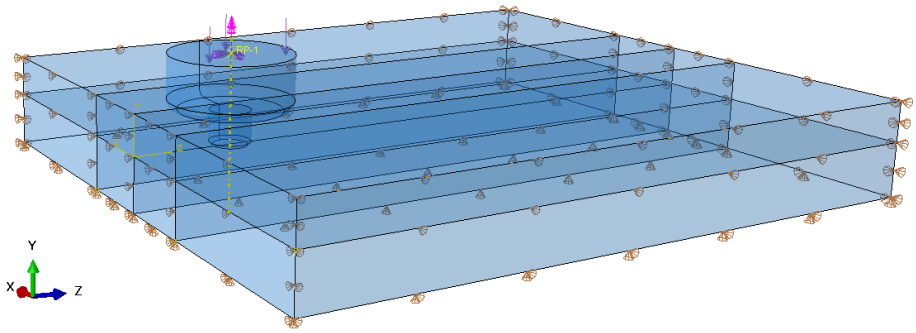

Fig. 2. Schematic diagram of boundary condition setting

In order to study the law that the quality of the weld is affected by the welding parameters, three groups of welding parameters: α, β and γ, were set in the simulation for comparative analysis. The welding parameters are set as follows:

Table 3.

Welding parameters of groups α, β and γ

welding parameters	α	β	γ
rotating speed（r/min）	793	1200	1200
Welding speed（mm/min）	240	240	144

3. Analysis and results

In this study, the thermodynamic coupling process of 7075 aluminum alloy FSW process was simulated based on CEL method. Focusing on the influence of temperature field, stress and strain of welded joint on weld forming quality, and drawing relevant curves to obtain intuitive data analysis. The results of numerical calculation predict the formation of defects after welding and explore the correlation of welding parameters to the formation of defects in 7075 aluminum alloy joints.

3.1 Analysis of weld morphology

The temperature nephogram of three stages: plunging, dwelling and welding is shown in Fig 3. As a result of the heat build-up effect during welding, it is observed that the total temperature of the material increases with the welding time[25]. In the first two stages of welding (Figure 3a, 3b), the temperature nephogram presents a classic "onion ring" shape, and the temperature distribution in the ring area is relatively symmetrical. After the shoulder is in contact with the upper surface of material and participates in friction heat generation, the heating rate of the plate increases significantly, and the temperature decreases from the stirring zone to the base material zone layer by layer.

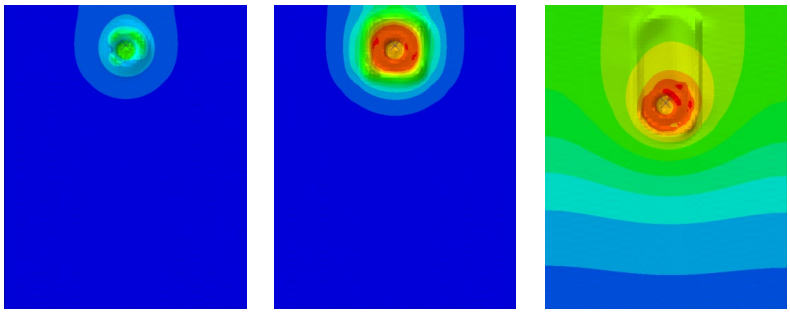

a) Plunging ***b***) Dwelling ***c***) Welding

Fig. 3. Temperature nephogram and weld formation in different welding stages

Fig. 4 and fig. 5 respectively show the temperature rise curve of a point in the highest temperature region of the retreating side (RS) and the flow forming effect of the joint material under different parameter conditions. Under welding conditions with a rotating speed of 794 r/min and a welding speed of 240 mm/min, respectively, the highest temperature of the selected point is 514℃. There are continuous and large tunnel defects on the advancing side (AS) of the joint, and the flash is obvious. When the rotating speed is increased to 1200r/min and the welding speed is unchanged, the maximum temperature is only increased to 524℃, and the defects of the joint tunnel are slightly reduced but not significant. From this, we

speculate that increasing the welding speed after some material reaches thermoplasticity can not effectively improve the heat input, and this phenomenon has been verified in existing research and experiments[14]. This is due to the viscosity of the material decreases at high temperature, which results in the decrease of friction between the stirring tool and the material. The energy consumption caused by continuously increasing the rotating speed does not match the improvement of welding effect. The weld quality was significantly improved when the rotating speed was kept at 1200r/min, the welding speed was reduced to 144mm/min, and the temperature increased to 568℃, that represent more than 93% of the melting point of 7075 aluminum alloy. As this time, the defect closure looks like discontinuous small holes, the welding flash is obviously reduced, and the welding surface becomes smooth.

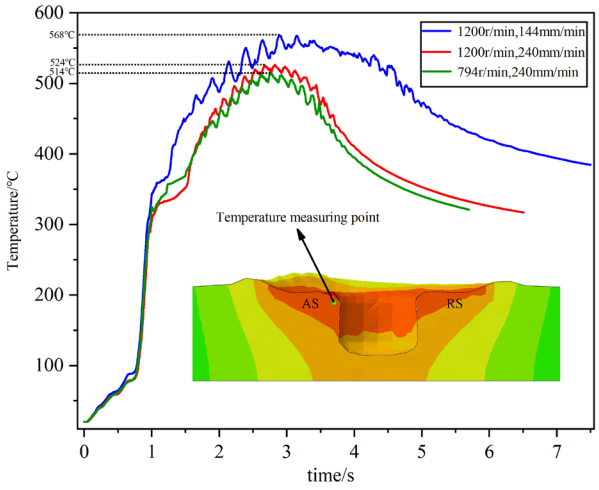

Fig 4. Temperature rise curves at different welding stages

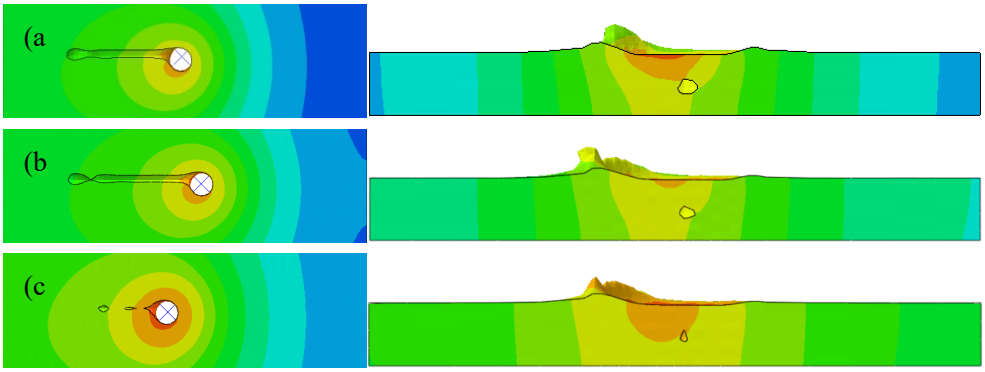

a) 794r/min,240mm/min b) 1200r/min,240mm/min c) 1200r/min,144mm/min

Fig. 5. Cross-sectional view of internal defects in weld simulation model

3.2 Experimental verification

In order to improve the reliability of the simulation results, FSW welding experiments were carried out with FSW-LM-L10 friction stir welding machine at rotating speed of 1200r/min and welding speed of 144mm/min and 240mm/min respectively, and then ultrasonic C-scan was used for nondestructive testing of the weld[26], and the results were compared with the simulation results. According to the weld morphology and C-scan diagram shown in Figure 6, it is found that there are obvious welding defects in the weld when the welding speed is 240mm/min, and when the welding speed is reduced to 144mm/min, the defects shrink and the abnormal parts are not obvious.

To sum up, the welding numerical analysis results in this paper are consistent with the experimental results, so the FSW simulation results are credible. The results show that when the rotating speed reaches about 794 r/min, it is of little significance to improve the weld quality by continuously increasing the rotating speed. Decreasing the welding speed can increase the heat input, make the material flow more fully and reduce the formation of internal defects in the weld. Adding grooves and threads to the stirring tool can improve the stirring ability, but it should be considered that more grooves and threads may reduce the strength of the stirring tool.

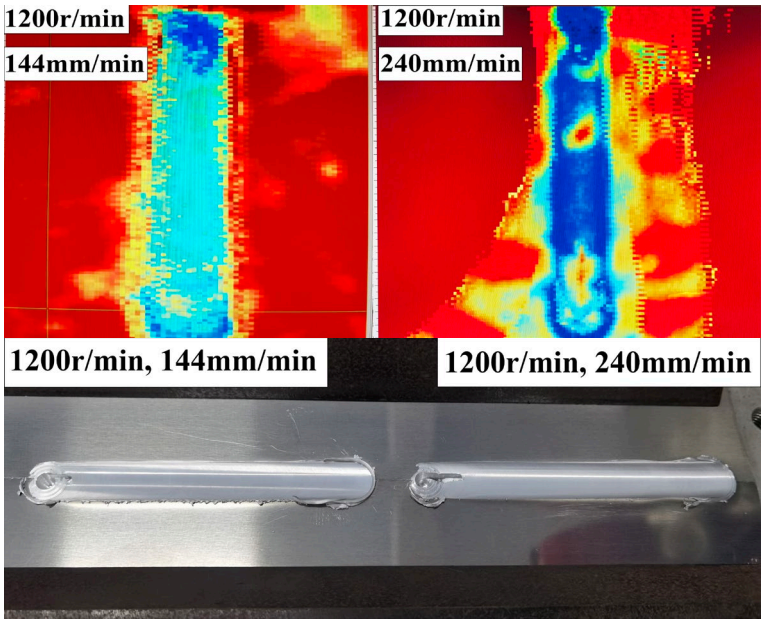

Fig. 6. Weld defects in the experiment

3.3 Analysis of weld temperature

When the welding proceeded to 6.3s, 20 uniform points were taken on the

upper surface and bottom surface of the material to form a circular path, and the temperature polar coordinate distribution curve was drawn (Fig. 7). According to the analysis curve, the distribution law of welding temperature on the upper and lower surfaces of the plate is approximately the same, and the temperature distribution is asymmetric during welding, which shows that RS temperature is obviously higher than AS. The highest temperature of the layer with the same thickness always appears behind the RS, which is caused by the stirring tool sweeping the thermoplastic material from the AS to the RS and accumulating behind the RS during welding. Fig. 8 is an axial sectional view of the weld during welding. In the thickness direction of aluminum plate, the temperature gradually decreases downward along the upper surface, and the nephogram shows an inverted cone shape, which proves that the extrusion and friction of shoulder are the main sources of heat generation during welding.

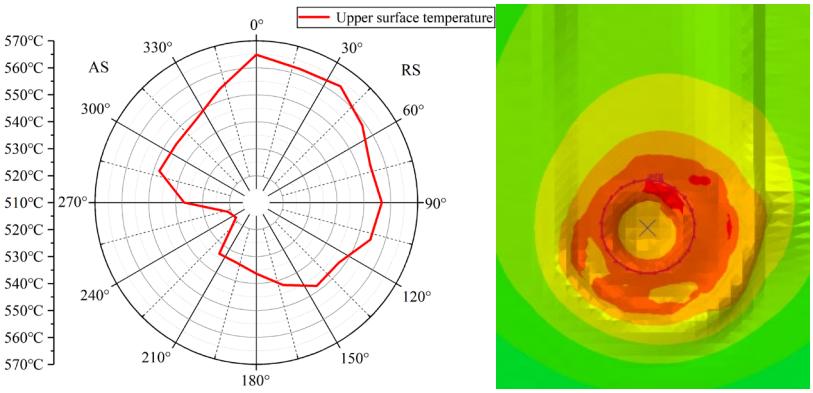

a) Upper surface temperature

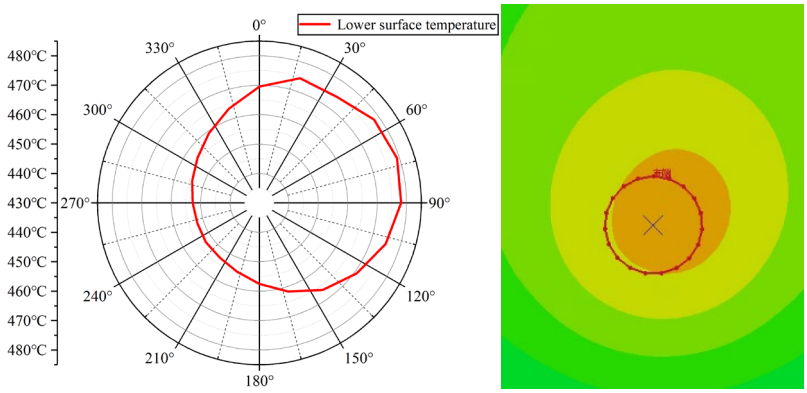

b) Lower surface temperature

Fig. 7. temperature polar coordinate curve

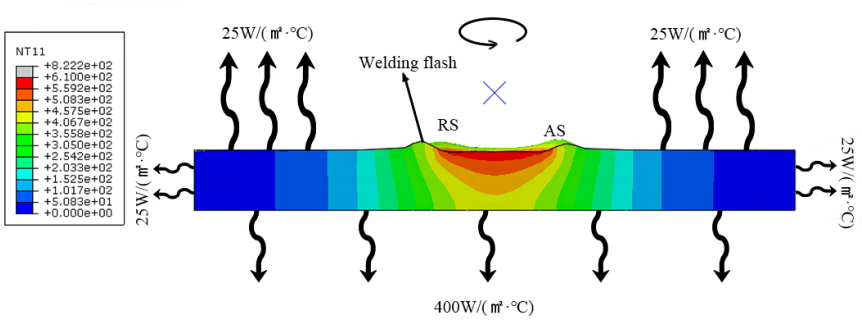

Fig. 8. Axial section of weld during welding

In addition to analyzing the temperature distribution at a certain moment, in order to study the trend of temperature change with time in the welding process, eight nodes, "A, B, C, D, E, F, G and H" are selected at different welding areas of the joint cross section of Scheme γ to draw temperature rise curves. For the convenience of comparison, the temperature rise curves are combined to draw the temperature change contrast curves of different welding areas, as shown in Fig. 9, and the position of the corresponding sampling point is shown in Fig. 10

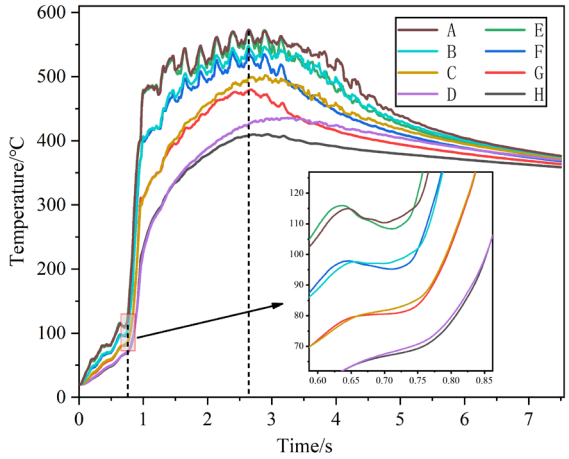

Fig. 9. Comparison curve of temperature change in different welding areas

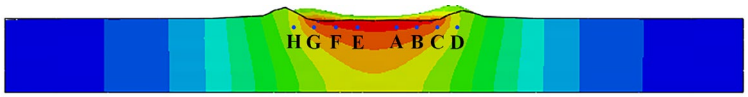

Fig. 10. Schematic diagram of curve point location

The analysis curve shows that the slope of the temperature rise curve increases sharply around 0.75s. At this time, the upper surface of the material bulges upward under the rotation and extrusion of the stirring pin, and friction occurs with the shaft shoulder to participate in heat generation. Subsequently, the stirring tool moves forward, and the slope of the temperature curve decreases, reaching the highest temperature in 2.65s. The highest temperature area is near point A, reaching

568℃, where the shoulder contacts the material on RS. The trend of temperature rise curves in different welding areas is basically the same.

The melting point of aluminum alloy 7075 is about 580~610℃. According to the temperature rise curve and weld forming results, it can be inferred that the temperature of Scheme γ has reached more than 93% of the melting point of the material, and sufficient thermoplastic materials have been produced, but there is still a phenomenon that the materials on the AS can not be replenished in time after being swept to the RS. Therefore, it is an effective measure to obtain excellent welds by using a lower welding speed to make the materials flow fully.

3.4 Stress and strain analysis

The stress distribution curve is shown in fig. 11a. Combined with the cross-sectional view of AS and RS stress nephograms (Fig. 12), it can be seen that stress variation trend of AS and RS is relatively consistent. Due to the extrusion of the stirring tool, the stress at the beginning and the end of the weld is high. Under the action of the stirring tool pushing forward and the fixture fixing, a Y-shaped stress zone is formed at the back end, which does not affect the performance of the welded joint. In the center of the weld, the stress always fluctuates between 100~200 MPa, and AS is slightly higher than RS, which is mainly the mechanical stress generated during welding and stirring.

The 3D stress model (Fig. 11b) can directly reflect the stress distribution in the cross section of the joint. Where "z" is the stress value, "x" is the distance from the weld center to the measuring point, and "y" is the distance from the lower surface of the material to the measuring point (expressed by the number of grids). From the model, it can be seen that the lower surface of the material is the part with greater stress, and the stress distribution in the welding process generally decreases with the increase of the distance from the measuring point to the weld center and the lower surface of the material.

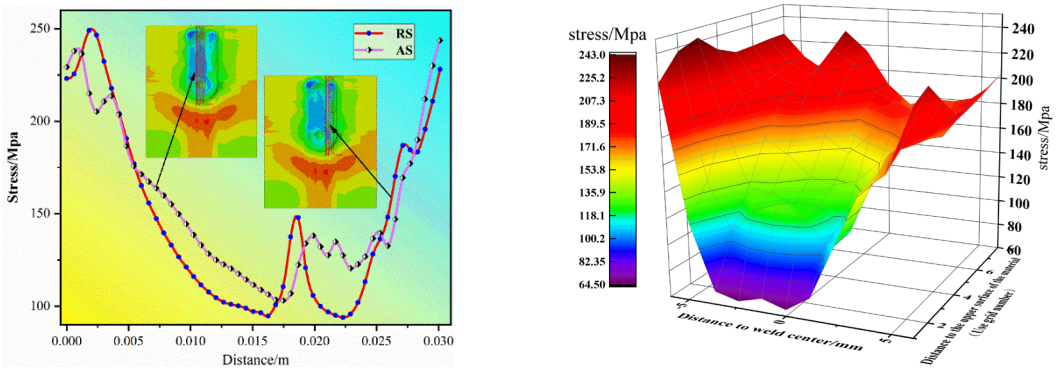

a) Stress distribution curve of upper surface of material

b) 3D model of stress distribution in weld cross section

Fig. 11. Stress distribution diagram

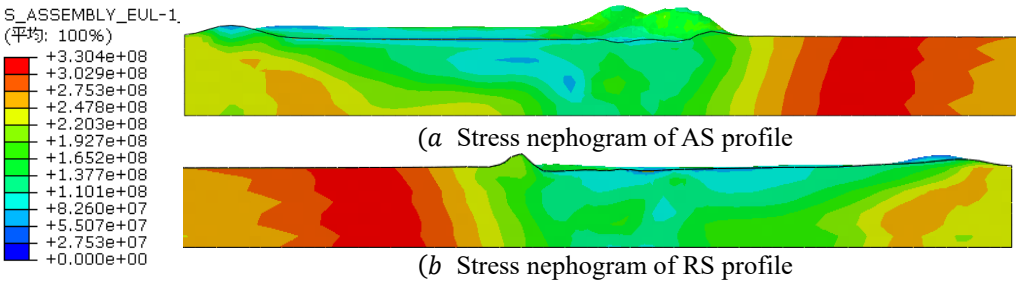

(*a* Stress nephogram of AS profile

(*b* Stress nephogram of RS profile

Fig. 12. Side sectional view of stress nephogram

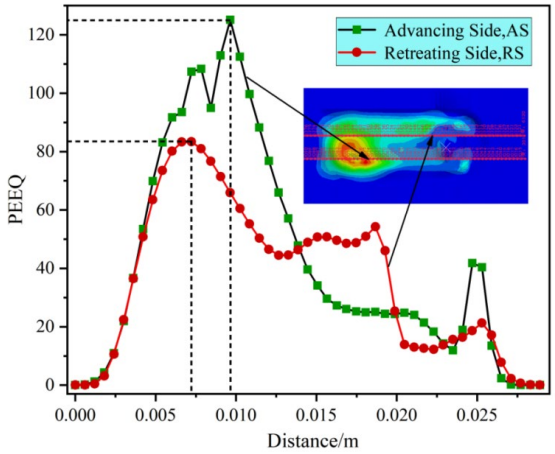

Fig. 13. PEEQ curves of AS and RS in the stirred area

By observing the equivalent plastic strain (PEEQ) nephogram (Figure 13) and comparing the PEEQ curves of AS (Advancing side, the side where the rotation direction of the stirring tool is the same as the welding direction) and RS (Retreating side, the side where the rotation direction of the stirring tool is opposite to the welding direction). It can be seen that the deformation of the beginning and end of the weld is more intense due to the extrusion and stirring of the stirring pin, and the PEEQ of AS and RS begins to differentiate after a short synchronous rise in the initial stage of welding, and the maximum PEEQ on the AS reaches about 122. However, in the center of the weld, the difference of PEEQ between AS and RS is small, and finally the RS is greater than AS. The material is swept from the AS to the RS and accumulated, so the flash on the RS is more obvious. The inconsistency of shape variables between AS and RS reflects the non-uniformity of material flow between them, which is an important basis for analyzing the causes of flash and defects.

4. Conclusion

This paper establishes a FSW process model for 7075 aluminum alloy based on the CEL method, and conducts research on temperature field around weld,

forming quality, and stress-strain. The following conclusions are drawn through research:

1) In the welding process, the shoulder is the main heat source. The temperature distribution in the welding area is asymmetric, which shows that the temperature of RS is higher than that of AS, and the highest temperature appears on the upper surface of the material in the mixing area inside the shoulder. Flash is mainly produced on the welding RS, and the internal defects of the weld are mainly distributed on the welding AS.

2) After the material reaches thermoplasticity, the continuous increase of rotating speed will lead to the waste of energy, and it is difficult to significantly improve the welding temperature. Proper reduction of welding speed can effectively increase the temperature, increase the transformation of thermoplastic materials and improve the forming quality of joints on the premise of saving energy. Under welding conditions with a rotating speed of 1200 r/min and a welding speed of 144 mm/min, respectively, the quality of the joint is good.

3) The distribution of stress and strain during welding is also an important factor affecting the joint forming. The weld stress distribution is relatively symmetrical, and the PEEQ distribution is uneven. The PEEQ in the stirring zone shows that AS is greater than RS at the beginning and end of the weld. But in the center of weld, it becomes that RS is greater than AS.

Funding

The author(s) disclosed receipt of the following financial support for the research, authorship, and/or publication of this article: Henan Province Science and Technology Research Project (No. 222102240017, 222102230049), Zhengzhou University of Aeronautics Graduate Education Innovation Program Fund Project (No.2023CX59) for their support to this research.

REFERENCES

[1]. *Kumar Rakesh, Singh Bhadauria Shailendra, Sharma Varun, et al*. Effect on microstructure and mechanical properties of single pass friction stir welded aluminium alloy AA-7075-T651 joint. Materials Today: Proceedings,2023,80(P1):40-47.

[2]. *Sarah Kleinbaum, Cindy Jiang, Steve Logan*. Advances in dissimilar metals joining through temperature control of friction stir welding. MRS Bulletin, 2019, 44(8):613-618.

[3]. *Zhen Zhang, Peng Xue, Dong Wang, et al*. Microstructure and mechanical properties of T-type friction stir welded SiCp/2009Al composite matrix material. Transactions of the China Welding Institution, 2022, 43(06):75-81+117-118.

[4]. *Meng Xiangchen, Huang Yongxian, Jian Cao, et al*. Recent progress on control strategies for inherent issues in friction stir welding. Progress in Materials Science, 2021, 115.

[5]. *Pengfei Yu, ChuanSong Wu, Lei Shi*. Analysis and characterization of dynamic recrystallization

and grain structure evolution in friction stir welding of aluminum plates. Acta Materialia, 2021, 207:116692.

[6]. *Kuritsyn D N, Siluyanova M V, Denisov L V, et al*. Durable Tools for Friction Stir Welding of High-Temperature Airplane-Engine Components. Russian Engineering Research, 2020, 40(6):497-500.

[7]. *Shtrikman M M, Kornevich P A, Pinskiy V A, et al*. Friction stir welding of ribbed panels of aircraft airframes. Welding International, 2018,32(3):219-222.

[8]. *Worood Hussein, Mohsin Abdullah Al-Shammari*. Fatigue and Fracture Behaviours of FSW and FSP Joints of AA5083-H111 Aluminium Alloy. IOP Conference Series: Materials Science and Engineering, 2018, 454(1).

[9]. *Andrade D, Leitão C, Dialami N, et al*. Modelling torque and temperature in friction stir welding of aluminium alloys. International Journal of Mechanical Sciences, 2020, 182(prepublish).

[10]. *Arunagiri Azhagar, Kunio Hayakawa*. Effects of Tool Surface Geometry on Temperature Distribution and Material Properties of an Aluminum Alloy in Friction Stir Welding. Materials Transactions, 2020, 61(2):276-281.

[11]. *Milcic D K J*. The influence of process parameters on the mechanical properties of friction-stir-welded joints of 2024 T351 aluminum alloys. Materiali in Tehnologije, 2019, 53(6).

[12]. *Mostafa A, Rahimi H A, MRM A*. Investigation of the effect of welding and rotational speed on strain and temperature during friction stir welding of AA5083 and AA7075 using the CEL approach. Engineering Research Express, 2023, 5(2).

[13]. *Salloomi K N*. Fully coupled thermomechanical simulation of friction stir welding of aluminum 6061-T6 alloy T-joint. Journal of Manufacturing Processes, 2019, 45:746-754.

[14]. *Khammass Hussein, S.*Analysis of the temperature distribution in friction stir welding of AA 2024-T3 and AA 6061-T6 using finite element method. UPB Scientific Bulletin, Series D: Mechanical Engineering, 2016, 78(4): 119-132.

[15]. *Gaoqiang Chen, Qingxian Ma, Shuai Zhang, et al*. Computational fluid dynamics simulation of friction stir welding:A comparative study on different frictional boundary conditions. Journal of Materials Science & Technology, 2018(1):128-134.

[16]. *Robe J*. R-ALE simulation of heat transfer during friction stir welding of an AA2xxx/AA7xxx joint on a large process window. International Journal of Mechanical Sciences, 2019, 155:31-40.

[17]. *Akbari M, Asadi P*. Dissimilar friction stir lap welding of aluminum to brass: Modeling of material mixing using coupled Eulerian–Lagrangian method with experimental verifications. Proceedings of the Institution of Mechanical Engineers, Part L: Journal of Materials: Design and Applications, 2020, 234(8):1117-1128.

[18]. *Akbari M, Asadi P, Behnagh A R*. Modeling of material flow in dissimilar friction stir lap welding of aluminum and brass using coupled Eulerian and Lagrangian method. The

International Journal of Advanced Manufacturing Technology, 2021, 113(3):1-14.

[19]. *Safari M, Joudaki J.* Coupled Eulerian-Lagrangian (CEL) Modeling of Material Flow in Dissimilar Friction Stir Welding of Aluminum Alloys. Shiraz University, 2019(2).

[20]. *Zhijian Nie, Yiming Qin, Jinhai Long, et al*. Microstructures performance and welding process of pulse TIG welded 7075 aluminum joints prepared with nano TiC aluminum matrix composite filler. Welding & Joining, 2023(04):29-36.

[21]. *Murat T, Özler K*. Numerical modeling of defect formation in friction stir welding. Materials Today Communications, 2022, 31.

[22]. *Salloomi K N, Al-Sumaidae S*. Coupled Eulerian-Lagrangian prediction of thermal and residual stress environments in dissimilar friction stir welding of aluminum alloys. Journal of Advanced Joining Processes, 2021, 3:100052.

[23]. *Zhi Zhu, Min Wang, Hui-jie Zhang, et al*. Simulation on material flow and defect during friction stir welding based on CEL method. The Chinese Journal of Nonferrous Metals, 2018, 28(02):294-299.

[24]. *Xiaoyan Wu, Wei Luo, Yisong Wang, et al*. Simulation on friction stir welding 7055 aluminum alloy based on CEL model. Transactions of the China Welding Institution, 2021, 42(07):44-50+59+100-101.

[25]. *Jiaqing You, Yunqiang Zhao, Miao Shu, et al*. Effects of welding physical fields on the microstructure evolution during dynamic-stationary shoulder friction stir welding. Journal of Materials Research and Technology, 2023, 23:3219-3231.

[26]. *Petriceanu, C., Rontescu, C., Cicic, D.-T. et al.* Research on welding of plastic materials. UPB Scientific Bulletin, Series D: Mechanical Engineering, 2016, 78(2): 125-130.